Journal of Power Sources 242 (2013) 762–767

Contents lists available at SciVerse ScienceDirect

Journal of Power Sources

journal homepage: www.elsevier.com/locate/jpowsour

First-principles study on the mechanism of coking inhibition by the Ni(111) surface doped with IB-group metals at the anode of solid oxide fuel cells

Pengju Zuo, Zhaoming Fu, Zongxian Yang*

College of Physics and Electronic Engineering, Henan Normal University, Xinxiang, Henan 453007, People's Republic of China

HIGHLIGHTS

- On pure Ni or IB metals (M), C-dimer configurations are preferred.
- On the Ni/M alloy, the separated C-atoms configurations are preferred.
- The C atoms tend to be adsorbed far away from the dopant atoms on Ni/M(111) surfaces.
- The M dopants in the Ni(111) enhance the energy barriers for the C-dimer formation.

GRAPHICAL ABSTRACT

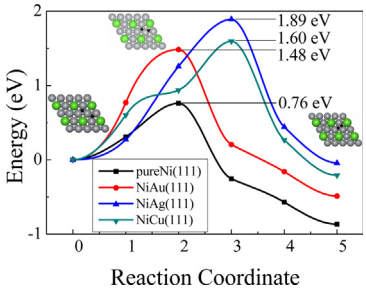

ARTICLE INFO

Article history:
Received 12 March 2013
Received in revised form
22 May 2013
Accepted 28 May 2013
Available online 6 June 2013

Keywords:
Solid oxide fuel cell
Nickel-based alloy anode
Adsorption energy
Density of states
Diffusion barrier

ABSTRACT

Focusing on the mechanisms of coking inhibition properties of the nickel-based alloy catalysts, the adsorption and diffusion of single C atoms and C dimer on the (111) surfaces of pure metals (Ni, Cu, Ag and Au), as well as the bimetallic systems (Ni/M) with 1/4 ML of M atoms in the surface layer of Ni(111) are studied based on spin-polarized density functional theory calculations, where M represents the IB metals (Cu, Ag and Au). It is confirmed that C atoms are energetically favorable to be adsorbed at the three-fold hollow sites on the pure Ni and M surfaces. Introducing M into Ni surface can weaken the adsorption of C due to the 3d-bands of the dopant atoms are farther from the Fermi level than those of Ni, which makes the three-fold hollow sites with IB dopant neighbor(s) unstable for carbon adsorption. The diffusion barriers for the process of C-dimer formation (C + C → C dimer) on the bimetallic surface are all higher than that on pure nickel. The results provide a proper explanation on the suppression effects of carbon deposition on the nickel-based alloy catalysts.

1. Introduction

Solid oxide fuel cells (SOFCs) are electrochemical devices that directly convert chemical energy from fossil fuel into electricity, and have attracted extensive attention due to their ability to achieve high energy conversion efficiencies and their inherent fuel flexibility. Ni–YSZ (Y_2O_3 stabilized ZrO_2) composites (cermets) are the most commonly used anodes in SOFC due to the high electronic conductivity and catalytic activity of Ni, and their ease of fabrication. While Ni–YSZ cermet anodes have these positive attributes, they suffer some serious drawbacks, such as low tolerance to hydrocarbon and sulfur impurities, which seriously influence the performance of SOFCs [1–5].

In the case of direct utilization of hydrocarbons as the fuel (called direct hydrocarbon SOFCs), which simplifies the SOFC systems and improves the efficiency by avoiding the use of external reformers [6], Ni also catalyzes some side reactions, e.g., the formation of carbon fibers [1,7]. While SOFCs in operation, carbon atoms generated by the accompanied side reactions will be

* Corresponding author. Tel.: +86 373 3329346.
E-mail addresses: yzx@henannu.edu.cn, zongxian.yang@163.com (Z. Yang).

0378-7753/$ – see front matter © 2013 Elsevier B.V. All rights reserved.
http://dx.doi.org/10.1016/j.jpowsour.2013.05.151

continuously absorbed and deposited on the catalyst surface. These carbon atoms may grow into carbon clusters such as graphene islands, which occupy the active sites of anode and impede the reactants to approach, and therefore lead to dropping of the catalytic activity of the anode catalysts [8], and a remarkable reduction of the cell performance [9–11]. Therefore the formation of carbon clusters (carbon deposition or coking) is an issue that limits the state-of-the-art Ni–YSZ material to be used in the direct hydrocarbon SOFCs. To resolve this issue, one strategy for the development of new anodes involves the use of bimetallic anodes, in which one metal is used as a catalyst, while the other provides the required carbon tolerance. For instance, many researchers are committed to improve the properties of Ni catalysts with the IB-group metallic dopants, (M = Cu, Ag and Au), e.g. using Ni/Cu [12,13], Ni/Ag [14–16] and Ni/Au [17] to replace pure Ni. Experimentally, it has been found that alloying the nickel catalyst with IB-group metals can largely eliminate the carbon deposition [14,17,18]. In particular, Ni/Ag was found to exhibit distinctive properties to eliminate the growth of filamentous carbon [14]. Although some theoretical studies have been performed [19,20], the mechanisms of coking inhibition are still obscure. For example, Zhang et al. [19] found that the pure IB-group metals are even more favorable to catalyze the formation of carbon clusters from carbon atoms than the pure Ni. Therefore, it is still difficult to illustrate the mechanism of coking inhibition through doping IB-group metals into the Ni catalysts.

In this work, we not only investigate the adsorptions of C atoms and C dimer on various pure metals or alloys, but also investigate the reaction processes from separated C atoms to carbon dimers. The adsorption energy for carbon on the surfaces of Ni, M and Ni/M alloy, together with the density of states (DOS) of the substrates and reaction barriers, are calculated. The results explain quite well the mechanism of coking inhibition of the Ni-based alloys with IB metal dopants. The paper is structured as follows. In Section 2, the computational method is detailed. The calculated adsorption energies of C adsorbates and the diffusion activation energies between separate C atoms and C dimer on different substrates and the comparison with previous experimental and theoretical data are given in Section 3. In Section 4, we conclude by discussing the implication of our results for understanding the effect of IB-group metal on the catalytic activity of Ni toward C adsorption and diffusion.

2. Models and calculation details

2.1. Models

The calculated lattice constant of bulk Ni is 3.52 Å, which is in good agreement with the previous theoretical [21] and experimental result of 3.52 Å [22]. The Ni(111) surface is shown in Fig. 1(a) and (b), which is built based on the calculated lattice constant of bulk Ni and represented by a supercell composed of a 4-layer slab with a p(2 × 2) surface and a vacuum space of 10 Å. The 4-layer slab was proved to be a good model due to the close-packed face-centered cubic (fcc) (111) surfaces [23], and a 10 Å [24,25] vacuum was found to be enough to simulated the surface. The pure IB metals are modeled similarly as the Ni(111). The IB metal atoms are introduced in the topmost layer of the Ni(111)-p(2 × 2) surface to build the surface alloy as shown in Fig. 1(c), Ni/M(111). The supercell models with the (2 × 2) and (4 × 4) surface replications are used to study the adsorption of a single carbon atom and the coadsorption of two separated carbon atoms, respectively. The migration of C atoms is simulated on the (4 × 4) supercell models as shown in Figs. 1(d) and 2. The free-standing C atoms and C dimer are simulated through a large cell with dimensions of 10 × 10 × 10 $Å^3$.

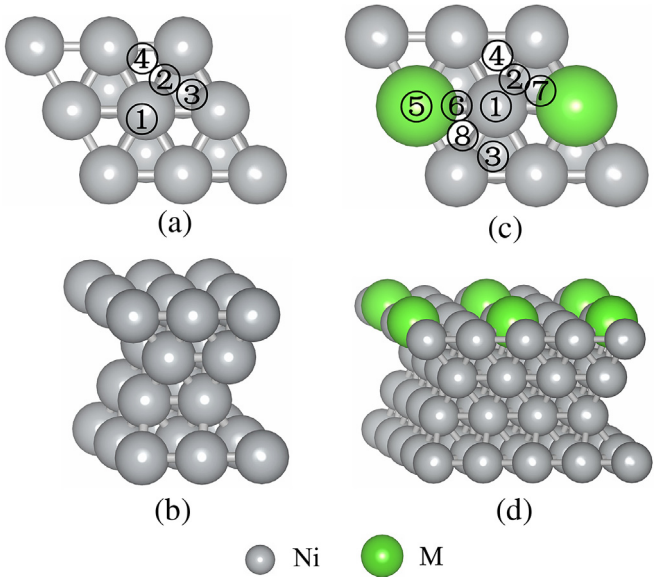

Fig. 1. Schematic representations of the adsorption sites on the (111) surfaces of (a) pure metals, Ni or M and (c) alloy, Ni/M. (a) ① top site; ② bridge site; ③ hcp site; ④ fcc site. (b) Side view of the 4-layer slab model of Ni/M system with a p(2 × 2) surface. (c) ① Ni top; ② Ni–Ni bridge; ③ hcp_{Ni} (hcp site surrounded by Ni atoms); ④ fcc_{Ni} (fcc site surrounded by Ni atoms); ⑤ M top; ⑥ Ni–M bridge; ⑦ hcp_{mix} (hcp site surrounded by two Ni atoms and one M atom); ⑧ fcc_{mix} (fcc site surrounded by two Ni atoms and one M atom). (d) Side view of the 4-layer slab model of Ni/M system with a p(4 × 4) surface.

For a (2 × 2) supercell, the top, hexagonal close-packed (hcp), face-centered cubic (fcc), and bridge sites are considered for the adsorption. Fig. 1(a) shows the schematic representations of the high symmetry sites (top, bridge, hcp, fcc) on the monometallic Ni(111) or M(111) surfaces. On the pure Ni or M surfaces, the environment of each site of the same kind is identical. However, in the case of Ni/M alloy, it varies due to the existence of two constituents in the lattice. The fcc_{Ni} and hcp_{Ni} are designated for the fcc and hcp sites surrounded by Ni atoms only, while the fcc_{mix} and hcp_{mix} for those surrounded by the both kinds of atoms in the top layer of the surface as shown in Fig. 1(c).

2.2. Calculation details

Spin-polarized calculations are performed using the Vienna Ab-Initio Simulation Package (VASP) [26,27]. The ionic cores are represented by the projector augmented wave (PAW) potentials [28]. The Kohn–Sham orbitals are expanded using plane waves with the well converged cutoff energy of 408 eV. Brillouin zone integrations are performed using Monkhorst–Pack grids [29] of 4 × 4 × 1 and 2 × 2 × 1 for the p(2 × 2) and the p(4 × 4) slab calculations, respectively. Our test calculations for the p(4 × 4) slab with MP grids of 4 × 4 × 1 gave almost the same adsorption energies and geometries as with the MP grids of 2 × 2 × 1.

Adsorbates are introduced on only one side of the slab. The leading errors induced by the existence of dipole moments in the supercells are corrected by using the methods as implemented in the VASP. The atoms in the top two layers are allowed to relax according to the atomic forces, while the atoms in the bottom two layers are fixed to the bulk positions to mimic the bulk.

The exchange and correlation interaction among electrons are described at the level of the generalized gradient approximation (GGA), using the Perdew–Burke–Ernzerhof (PBE) formula [30]. The Gaussian smearing [31] method is employed to determine electron occupancies with a smearing parameter σ of 0.2 eV.

The convergence criteria for the electronic self-consistent iteration and the ionic relaxation loop are set to 10^{-5} eV and 0.02 eV Å^{-1}, respectively.

The adsorption energies, E_{ad}, are calculated as

$$E_{ad} = E_{adsorbate/sub} - E_{adsorbate} - E_{sub},$$

where $E_{adsorbate/sub}$, $E_{adsorbate}$ and E_{sub} represent the total energies of the optimized substrate with adsorbate, the isolated adsorbate molecule, and the clean surface, respectively. A negative E_{ad} represents the exothermic adsorption, and the greater the magnitude of E_{ad} means the stronger binding of the adsorbate to the surface.

The climbing-image nudged elastic band (CI-NEB) [32–34] method is used to locate the minimum energy paths (MEP) and transition states for carbon diffusion on the surfaces. A number of intermediate images are constructed along the reaction path between the energetically favorable reactants and products. In order to obtain accurate forces, the total energies are converged to within 1×10^{-5} eV per atom during the electronic optimization. Such a calculation is computationally demanding because of the high precision and large numbers of ionic relaxation steps for each image along the reaction path. Based on the comparison of the energy barriers on different surfaces, we conclude by discussing the implication of our results for understanding the effect of M introduction upon the C diffusion and coking inhibition. We try to use the international system of units (SI) in this paper. However, we keep some of the popular units used in the micro world and give their equivalent in SI for clarity, e.g., 1 eV = 1.60217733 $\times$ 10^{-19} J; 1 Å = 10^{-10} m; 1 e = −1.60217733 $\times$ 10^{-19} C and 1 eV Å^{-1} = 1.60217733 $\times$ 10^{-9} N.

3. Results and discussion

3.1. Adsorption energy

In the process of carbon deposition on the Ni–YSZ anode, atomic carbon adsorption is one of the key steps. Therefore, adsorption energy calculation on the cermet anode is a convenient way to identify potential carbon-tolerant metallic catalysts in the anode. The metals with higher adsorption energies for atomic carbon are more susceptible to the carbon deposition for the anodes using hydrocarbon fuels. The calculated adsorption energy of atomic C on the (111) surfaces of Ni, M and Ni/M alloy are summarized in Fig. 3 and Table 1. It is found that carbon atom preferentially adsorbs on the three-fold hollow sites (hcp and fcc sites on the Ni(111); hcp_{Ni} and fcc_{Ni} sites on the Ni/M(111)) surrounding with three Ni atoms and forms three equivalent C–Ni bonds of 1.77 Å on the p(2 $\times$ 2) Ni(111) and Ni/M(111) surfaces. The C atoms on all the top and bridge sites of Ni(111) and Ni/M(111) surfaces are not stable and move to the neighboring hcp sites after geometry optimization. Specifically, on the Ni/M(111) surface, the C atoms at the three-fold hollow sites neighboring dopant atoms (hcp_{mix} or fcc_{mix} sites) are not stable, and move to the neighboring three-fold hollow sites surrounded by Ni atoms (hcp_{Ni} and fcc_{Ni} sites) only. Therefore, the most stable adsorption sites of C adatoms on the Ni/M(111) surfaces are the three-fold hollow sites surrounded by Ni atoms. While adsorbed on the hollow sites, the height of the C atom (h_C, the vertical distance between the C atom and the top layer of the substrate Ni/M(111) surface) is determined to be 0.99 Å, which is significantly smaller than that for C on the top site of M (1.83 Å) due to the difference in coordination number. The same tendency is

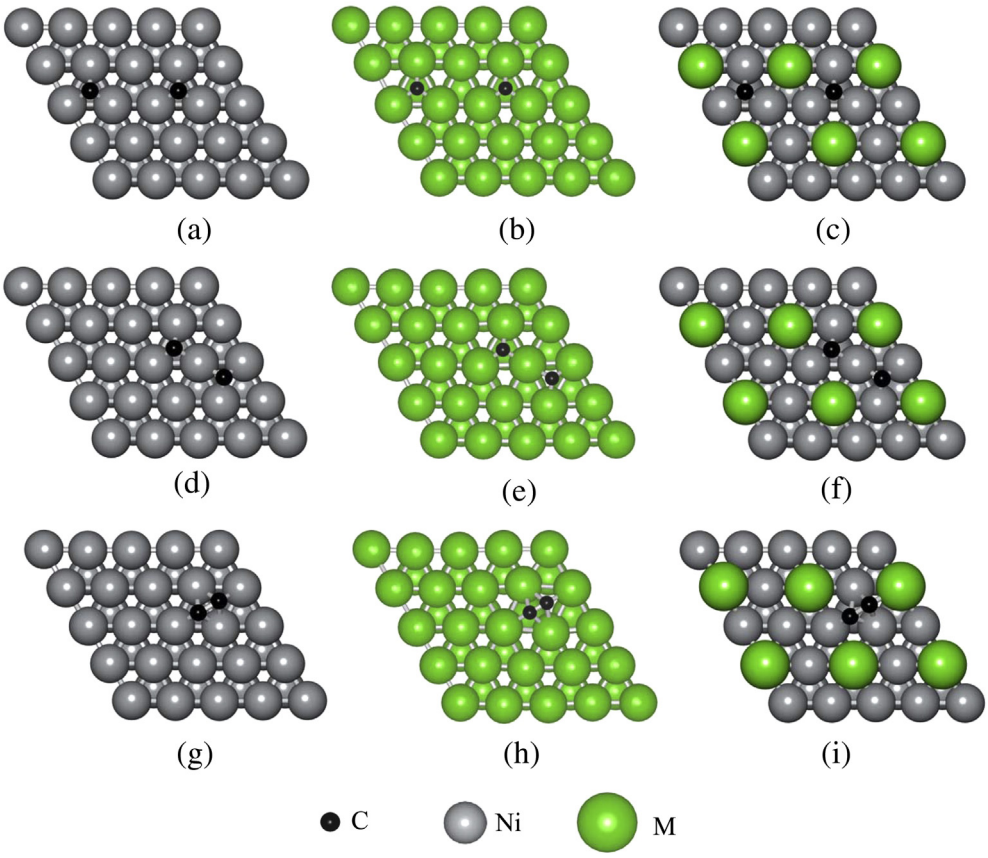

Fig. 2. Top views for the configurations of two separated C atoms (a–f) and C dimer (g–i) adsorbed on the (111) surfaces of Ni, M and Ni/M. Structures a–c are the most stable configurations, and structures d–f are the metastable ones.

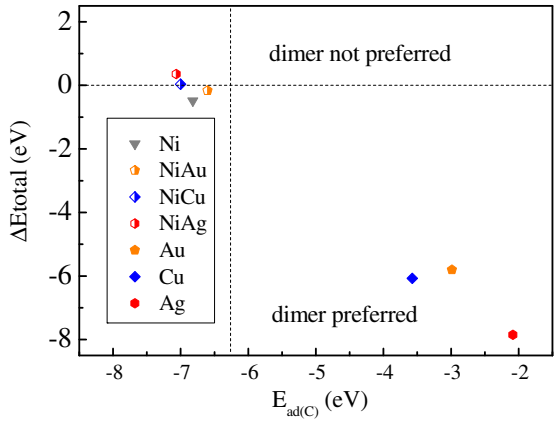

Fig. 3. Total energy difference between the configurations of a C dimer ($E_{Cdimer/substrate}$) and two separate C adatoms ($E_{2singleC/substrate}$) with respect to the adsorption energy for atomic C, $E_{ad(C)}$, on (111) surfaces of Ni, M and Ni/M. Vertical dashed line corresponds to the binding energy of a C–C double bond (−6.33 eV) [38] in a free C_2 molecule.

also observed for C adsorption on Ni(111) and M(111) surface, suggesting that the h_C values are related to the adsorption energies, i.e., a smaller value of h_C corresponds to a more negative adsorption energy. On both the Ni(111) and M(111) surfaces, a C atom prefers to be adsorbed on the three-fold hollow sites (fcc and hcp) with a smaller h_C rather than on the top site. Comparing the adsorption energies on these metal surfaces, it is concluded that the adsorption stability of C atoms on the Ni(111) surface is higher than those on the M(111) surfaces. For the alloyed Ni/M(111) surface, a C atom prefers to be adsorbed on the three-fold hollow sites (fcc_{Ni} and hcp_{Ni}) surrounded by Ni atoms, which demonstrates again that the Ni atoms have a larger attractive tendency to the C adatom than the IB metals. The hcp_{mix} and fcc_{mix} referred in Fig. 1 are not the stable adsorption sites of C atoms. The initial C atoms on these sites would spontaneously move to the three-fold hollow sites composed by three Ni atoms after the structure optimization. The calculated adsorption energies are shown in Table 1, in agreement with the result of the previous work [35].

Chen et al. [19] pointed out that, for the adsorption of C atoms on metals, a weaker C-metal interaction would correspond to a higher tendency for C-dimer configurations. Their calculated results also suggested that C atoms are all dimer preferred on the surfaces of IB-group metals, and Ni is on the threshold between the dimer preferred systems and the dimer not preferred ones. In this work, the similar calculations for the adsorption of C atoms on the Ni/M alloy surfaces are performed to investigate the characters of Ni/M(111) surface. Generally, the interactions involved in the coadsorption system can be divided into two parts: the adsorbate–substrate interaction and the adsorbate–adsorbate interaction. Therefore, as the adsorbed C atoms are combined into dimers (C_2), the two kinds of interactions are both changed. The former becomes weaker due to the modification of electronic structure, and the latter becomes stronger due to the C–C bond formation. The net effects of the two factors are responsible for the stability of the adsorption systems. If the net effects lead to the reduction in total energy, the reaction from two adsorbed C atoms to C_2 is exothermic and the substrates would be dimer preferred. According to the total calculations, the separated C configurations are preferred on the Ni/M alloys though the C-dimer ones are preferred on the pure Au, Ag and Cu, which means that the C_2 formation on alloys is endothermic, while that on pure the metals is exothermic. As mentioned, while two adsorbed C atoms bind together and turn to a dimer on pure Ni, the Ni–C binding will be weakened with the formation of C–C bond, as shown in Table 2. The former corresponds to energy enhancement and the latter corresponds to energy reduction. The net effects result in the reduction of total energy. Therefore the pure metals prefer C-dimer adsorption. However, on the alloy surfaces the situation is different. The reason is that some Ni–C bonds are replaced by the weaker M–C bonds (M = Au, Ag and Cu), which is in favor of the dimer formation, as shown in Table 2. And on the surface doped with 25% dopants M (M = Au, Ag and Cu), the dimers are bound to bind with dopant atoms, which lead to the reduction of adsorption stability, as shown in Fig. 2(i). In contrast, the separated C atoms can be adsorbed on hcp_{Ni} sites binding with Ni atoms only, as shown in Fig. 2(c) and (f). The results in Table 2 indicate the difference of C–M bond energy and C–Ni bond energy. We calculated the adsorption energies of a C dimer on the monometallic Ni(111) and M(111) surfaces, and defined the mean bond energy of Ni–C and M–C bonds of the adsorption system of C_2 (Fig. 2(h) and (i)) and 2C (Fig. 2(a) and (b)). The mean bond energy (E_{bond}) is defined by

$$E_{bond} = E_{ad}/N_{bonds},$$

where E_{ad} is the adsorption energy of C adsorbates (2C or C_2) on different surfaces and N_{bonds} represents the total number of Ni–C and M–C bonds.

Since the C–Ni interaction is stronger than the C–M, the C dimer will be pulled closer to the hcp_{Ni} sites and further from the M atoms, so that the neighboring atoms are all Ni. Therefore, the bond symmetry of the C atoms in the C dimer will be broken, which leads to the mismatch of graphene growth on the Ni/M(111) surface. This will be quite significant to inhibit carbon deposition, i.e., the Ni/M(111) will not be suitable for graphene growth. Compared to the adsorption energy on the Ni(111) surface, we can see that the introduction of M can effectively reduce the tendency of C-dimer formation.

The adsorption energy of a C atom, $E_{ad(C)}$ is defined by $E_{ad(C)} = E_{C/sub} - E_C - E_{sub}$, where $E_{C/sub}$ and E_{sub} represent the total energies of the optimized substrate with and without the C adsorbate, respectively, while E_C represents the total energy of an isolated C atom. The total energy differences between configurations of a C dimer and two separated carbon atoms reflect the enthalpies of dimer formation reactions and are defined as:

$$\Delta E_{total} = E_{Cdimer/substrate} - E_{2singleC/substrate}$$

where $E_{Cdimer/substrate}$ is the total energy of the C-dimer configuration, and $E_{2singlC/substrate}$ is that of the configuration with two separated carbon adatoms. Therefore, the smaller the ΔE_{total} is, the

Table 1
Adsorption energies (in eV) of single C atom on the Ni/M(111) surfaces with the fcc_{Ni} and hcp_{Ni} configurations, respectively. The values in the parentheses are those on the M(111) surfaces with the fcc and hcp configurations.

Adsorption sites	Ni(111)	Ni/Au(111)	Ni/Ag(111)	Ni/Cu(111)
fcc_{Ni}	−6.76	−6.56 (−3.00)	−7.03 (−2.09)	−6.96 (−3.58)
hcp_{Ni}	−6.82	−6.60 (−2.80)	−7.07 (−2.01)	−7.00 (−3.52)

Table 2
Adsorption energy (in eV) for the configurations of C_2 and 2C, respectively. The values in parentheses are mean bond energy of the Ni–C and M–C bonds.

Substrates	C_2	2C
Ni(111)	−7.17 (−1.20)	−13.61 (−2.27)
Au(111)	−4.82 (−0.80)	−8.61 (−1.43)
Ag(111)	−5.06 (−0.84)	−7.61 (−1.27)
Cu(111)	−6.27 (−1.04)	−10.76 (−1.79)

more stable the dimer configuration. On the Ni(111) surface, the C dimer is more stable than the separated configuration due to the formation of C–C bond. On the bimetallic Ni/M(111) surfaces, two opposite factors exist. On the one hand, the C–C bond formation reduces the total energies. On the other hand, some of C–Ni bonds are replaced by the weaker C–M (M = Au, Ag and Cu) bonds. Therefore, it might be possible that the C-dimer configuration on Ni/M(111) is higher in energy than the separate configuration. Indeed, on the Ni/M(111) surfaces the C-atoms adsorption are not dimer preferred. In addition, the three-fold hollow sites neighboring the dopants are unstable to accommodate C atoms, indicating that the alloy surface can partially block the active sites for C adsorption. Therefore the alloyed surfaces cannot provide a large ensemble of active sites for the growth of graphene. These results demonstrate that Ni/M catalysts have high resistance to coke deposition.

3.2. Electronic structure

To have a better insight into the interactions between the adsorbates and surfaces, the partial density of states (PDOS) of the d-orbitals of the four metal atoms neighboring the adsorbed C dimer is calculated and shown in Fig. 4. Obviously, comparing with the 3d-bands of the dopant atoms, those of Ni are fairly close to the Fermi level, which is responsible for the stronger adsorption of C on the Ni(111) surface than those on the M(111) surfaces. As for the alloy surfaces, the differences of the PDOS near the Fermi energy are not quite distinct. Therefore the d-band centers of all surfaces are calculated, and the results are listed in Table 3, which suggest that the d-band centers of substrates are farther from the Fermi level as the dopants are introduced, which are in accordance with the PDOS as shown in Fig. 4, and could also explain the weaker adsorption of C on the Ni/M(111) surfaces than on the monometallic nickel surface. It can be concluded that the adsorption strength of C on the three categories of surfaces is in the order of Ni > Ni/M alloy > M, which is in agreement with the results of the adsorption energies. The addition of the M can weaken the activity of Ni and lowers the adsorption energy of atomic C. The metals that adsorb C atoms more strongly are more likely to be poisoned by carbon deposition. Therefore, the Ni/M alloys may serve as good carbon-tolerant anodes.

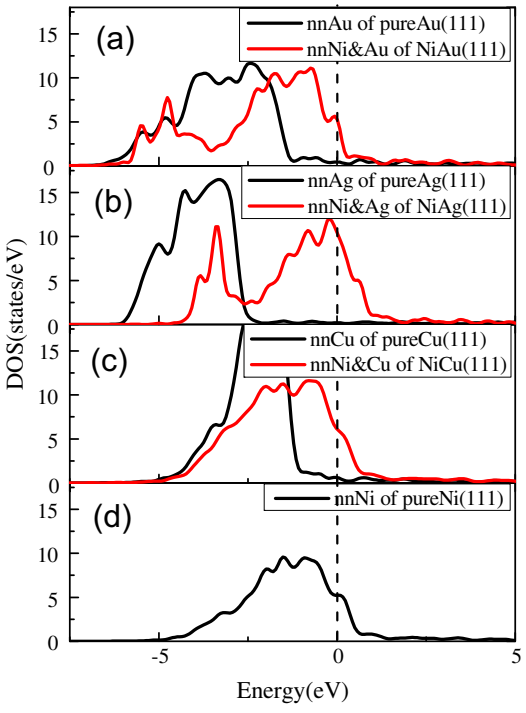

Fig. 4. PDOS (partial density of states) of the metal atoms neighboring C adsorbates on different surfaces, nnNi & nnM represent the neighboring metal atoms for the systems of (a) pure Au (black) and Ni/Au (red), (b) pure Ag (black) and Ni/Ag (red), (c) pure Cu (black) and Ni/Cu (red), and (d) pure Ni. (For interpretation of the references to color in this figure legend, the reader is referred to the web version of this article.)

Table 3
The d-band centers (in eV) of the metal atoms neighboring the C adsorbates in the pure Ni and the Ni/M systems. The values in the parentheses are those in the pure M(111) surfaces.

Metal atoms	Ni(111)	Ni/Cu(111)	Ni/Ag(111)	Ni/Au(111)
d-Band center	−1.16	−1.28 (−2.01)	−1.65 (−3.64)	−1.66 (−2.92)

3.3. Reaction barriers

The carbon deposition roots in the formation of carbon clusters, which can block the active sites on the catalysts. Therefore it is significant to investigate the growth of C clusters on the anodes. In this work, only the formation of C dimer is taken into account, which is the first step for C cluster growth.

For the formation of the C dimer, the entire reaction course includes two steps. The first step is the process from the most stable coadsorption structure to the metastable coadsorption structure by the diffusion of one C atom; and the second step is the transition from the metastable coadsorption structure to C-dimer structure. Because the diffusions of C atoms on the surfaces have been studied extensively [36,37], we focus on the second step with the formation of C dimer. The metastable adsorption structures as shown in Fig. 2(d) and (f) are therefore selected as the initial states of the transition. The systems with C dimers as shown in Fig. 2(g) and (i) are regarded as the final states. The corresponding transition states are calculated by the CI-NEB method [32–34] and the calculated minimum energy paths (MEP) are shown in Fig. 5. The results indicate that the activation energy for C-dimer formation is increased largely with the introduction of M dopants into the Ni(111), and the C atoms deposited on the catalyst surface can be readily separate into single atom by the M dopants. These separated C atoms are more easily to be oxidized and moved away [16]. These findings of kinetic analysis provide a rational interpretation for the experimental observations that the Ni/M catalysts exhibit high resistance to coke deposition.

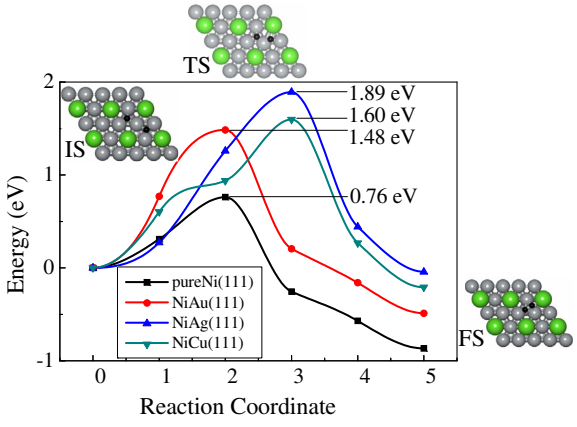

Fig. 5. The calculated minimum energy paths (MEP) with energy barriers denoted for surface diffusion between 2 separate C atoms and C dimmer.

4. Conclusion

Density functional theory calculations are performed for the adsorption of C atom and C dimer, as well as the energy barriers for the transition from the separated C configuration to the C-dimer configuration on different metal surfaces. The following conclusions are arrived.

Firstly, the C–Ni bond is stronger than the C–M bonds (M = Au, Ag and Cu) due to the 3d-bands of Ni are closer to the Fermi level than those of the dopant atoms, which is responsible for the stronger adsorption of C on the Ni(111) surface than those on the M(111) surfaces. Alloying Ni with the M dopants lowers the tendency for the formation of C dimer, which is responsible for coking inhibition by the Ni catalysts doped by IB-group metals. Secondly, on the Ni/M(111) surfaces, C atoms prefer to be adsorbed at the hcp sites with Ni neighbors only. Therefore, the introduction of dopants M results in losing of some of the active adsorption sites for C atoms. Lastly, the activation barriers for the C-dimer formation are enhanced with the introduction of M dopants into Ni(111). These findings provide a rational interpretation for the experimental observations that the Ni/M catalysts exhibit higher resistance to coke deposition than the pure Ni catalyst.

Acknowledgment

This work is supported by the National Natural Science Foundation of China (Grant Nos. 11174070 and 11247012) and the high-performance computing center of College of Physics and Electronic Engineering, Henan Normal University.

References

[1] M.L. Toebes, J.H. Bitter, A.J. Van Dillen, K.P. de Jong, Catalysis Today 76 (2002) 33–42.
[2] C. Toh, P. Munroe, D. Young, K. Foger, Materials at High Temperatures 20 (2003) 129–136.
[3] H. Kim, C. Lu, W. Worrell, J. Vohs, R. Gorte, Journal of the Electrochemical Society 149 (2002) A247–A250.
[4] Y. Matsuzaki, I. Yasuda, Solid State Ionics 132 (2000) 261–269.
[5] D. Sarantaridis, A. Atkinson, Fuel Cells 7 (2007) 246–258.
[6] S. McIntosh, R.J. Gorte, Chemical Reviews-Columbus 104 (2004) 4845–4866.
[7] T. Kim, G. Liu, M. Boaro, S.I. Lee, J.M. Vohs, R.J. Gorte, O. Al-Madhi, B. Dabbousi, Journal of Power Sources 155 (2006) 231–238.
[8] J.H. Koh, Y.S. Yoo, J.W. Park, H.C. Lim, Solid State Ionics 149 (2002) 157–166.
[9] K. Nikooyeh, R. Clemmer, V. Alzate-Restrepo, J.M. Hill, Applied Catalysis A: General 347 (2008) 106–111.
[10] H. Timmermann, W. Sawady, D. Campbell, A. Weber, R. Reimert, E. Ivers-Tiffee, Journal of the Electrochemical Society 155 (2008) B356–B359.
[11] Y. Lin, Z. Zhan, J. Liu, S.A. Barnett, Solid State Ionics 176 (2005) 1827–1835.
[12] W. An, X.C. Zeng, C.H. Turner, The Journal of Chemical Physics 131 (2009) 174702.
[13] R.J. Gorte, S. Park, J.M. Vohs, C. Wang, Advanced Materials 12 (2000) 1465–1469.
[14] N. Parizotto, K. Rocha, S. Damyanova, F. Passos, D. Zanchet, C. Marques, J. Bueno, Applied Catalysis A: General 330 (2007) 12–22.
[15] Y.A. Zhu, D. Chen, X.G. Zhou, P.O. Astrand, W.K. Yuan, Surface Science 604 (2010) 186–195.
[16] Y. Xu, C. Fan, Y.A. Zhu, P. Li, X.G. Zhou, D. Chen, W.K. Yuan, Catalysis Today (2011).
[17] N.C. Triantafyllopoulos, S.G. Neophytides, Journal of Catalysis 239 (2006) 187–199.
[18] G. Bonura, C. Cannilla, F. Frusteri, Applied Catalysis B: Environmental 121–122 (2012) 135–147.
[19] H. Chen, W. Zhu, Z. Zhang, Physical Review Letters 104 (2010) 186101.
[20] L. Jia, X. Wang, B. Hua, W. Li, B. Chi, J. Pu, S. Yuan, L. Jian, International Journal of Hydrogen Energy 37 (2012) 11941–11945.
[21] D.W. Blaylock, T. Ogura, W.H. Green, G.J.O. Beran, The Journal of Physical Chemistry C 113 (2009) 4898–4908.
[22] C. Kittel, P. McEuen, Introduction to Solid State Physics, Wiley, New York, 1996.
[23] C. Fan, Y.A. Zhu, Y. Xu, Y. Zhou, X.G. Zhou, D. Chen, The Journal of Chemical Physics 137 (2012) 014703.
[24] C. Dong, L. An, Y. Yang, J. Zhang, in: IEEE (2010), pp. 1–4.
[25] N.K. Das, T. Shoji, Applied Surface Science 258 (2011) 442–447.
[26] G. Kresse, J. Furthmüller, Computational Materials Science 6 (1996) 15–50.
[27] G. Kresse, J. Furthmüller, Physical Review B 54 (1996) 11169.
[28] G. Kresse, D. Joubert, Physical Review B 59 (1999) 1758.
[29] H.J. Monkhorst, J.D. Pack, Physical Review B 13 (1976) 5188–5192.
[30] J.P. Perdew, K. Burke, M. Ernzerhof, Physical Review Letters 77 (1996) 3865–3868.
[31] M. Methfessel, A. Paxton, Physical Review B 40 (1989) 3616.
[32] B.J. Berne, G. Cicootti, D.F. Coker (1998).
[33] G. Henkelman, B.P. Uberuaga, H. Jónsson, The Journal of Chemical Physics 113 (2000) 9901.
[34] G. Henkelman, H. Jonsson, The Journal of Chemical Physics 113 (2000) 9978–9985.
[35] L. Jia, X. Wang, B. Hua, W. Li, B. Chi, J. Pu, S. Yuan, L. Jian, International Journal of Hydrogen Energy (2012).
[36] Y.H. Shin, S. Hong, Applied Physics Letters 92 (2008) 043103.
[37] Y.A. Zhu, Y.C. Dai, D. Chen, W.K. Yuan, Surface Science 601 (2007) 1319–1325.
[38] L.G. Wade, sixth ed., Pearson Prentice Hall, Upper Saddle River, NJ, 2006, p. 279.